Annals of Mathematical Sciences and Applications
Volume 4, Number 1, 55–79, 2019

Matrix representations of discrete differential operators and operations in electromagnetism

Tsung-Ming Huang, Wen-Wei Lin, and Weichung Wang

Metamaterials with periodic structures are building blocks of various photonic and electronic materials. Numerical solutions of three dimensional Maxwell's equations, play an important role in exploring and design these novel artificial materials. Yee's finite difference scheme has been widely used to discretize the Maxwell equations. However, studies of Yee's scheme from the viewpoints of matrix computation remain sparse. To fill the gap, we derive the explicit matrix representations of the differential operators $\nabla\times$, $\nabla\cdot$, ∇, ∇^2, $\nabla(\nabla\cdot)$, and prove that they satisfy some identities analogous to their continuous counterparts. These matrix representations inspire us to develop efficient eigensolvers of Maxwell's equations and help to show the divergence free constraints hold in Yee's scheme.

Keywords and phrases: Maxwell's equations, Yee's discretization scheme, matrix representation, curl, divergence, gradient, periodic structures, simple cubic lattice, face centered cubic lattice.

1. Introduction

Propagations of electromagnetic waves in bianisotropic media can be, mathematically, modeled by the three dimensional (3D) Maxwell's equations

$$\nabla \times E(\mathbf{x}) = \iota\omega B(\mathbf{x}), \tag{1a}$$

$$\nabla \times H(\mathbf{x}) = -\iota\omega D(\mathbf{x}), \tag{1b}$$

$$\nabla \cdot B(\mathbf{x}) = 0, \tag{1c}$$

$$\nabla \cdot D(\mathbf{x}) = 0, \tag{1d}$$

where ω is the frequency, E, H, D and B are electric, magnetic fields, dielectric and magnetic flux densities, respectively, at the position $\mathbf{x} \in \mathbb{R}^3$. Furthermore, E, H, D and B satisfy the constitutive relations

$$B = \mu H + \zeta E \quad \text{and} \quad D = \varepsilon E + \xi H, \tag{2}$$

in which μ is the magnetic permeability, ε is the electric permittivity, and ζ and ξ are magnetoelectric coupling parameters. Materials modelled by Eq. (1) can be characterized by μ and ε as follows [15].

- $\mu > 0$, $\varepsilon > 0$, and $\zeta = \xi = 0$. Most dielectric materials belong to this category. The governing equations in (1) can be reformulated as

$$\nabla \times \mu^{-1} \nabla \times E = \omega^2 \varepsilon E, \quad \nabla \cdot (\varepsilon E) = 0,$$

  where ε is a material-dependent piecewise constant function.
- $\mu > 0$ and $\varepsilon < 0$. This category includes dispersive metallic materials, ferroelectric materials, and doped semiconductors. In dispersive metallic materials [3, 4, 5, 16, 17, 22], ε is not a piecewise constant but dependents on the frequency ω, that is, $\varepsilon = \varepsilon(\mathbf{x}, \omega)$. Such materials can exhibit negative permittivity at certain frequencies, such as below the plasma frequency.
- $\mu < 0$ and $\varepsilon < 0$. This category represents the left-handed material or negative-index materials. It is worth mentioning that there is no such material in nature. To demonstrate the material properties including the negative refractive index, artificial metamaterials with periodic structures have been proposed in [18, 19] firstly. Such metamaterials open up a completely new research area. For example, bi-isotropic and bianisotropic media are two important classes of metamaterials [23]. The associated B and D satisfy (2) (see [20, p. 26], [23, p. 44], for details).
- $\mu < 0$ and $\varepsilon > 0$. This category consists of some ferrite materials with negative permeability. However, the induced magnetic response fades away quickly above microwave frequencies.

Furthermore, for periodic structures, the Bloch Theorem [14] requires that the electric and magnetic fields E and H satisfy the quasi-periodic conditions

$$E(\mathbf{x} + \mathbf{a}_\ell) = e^{\iota 2\pi \mathbf{k}\cdot\mathbf{a}_\ell} E(\mathbf{x}), \ H(\mathbf{x} + \mathbf{a}_\ell) = e^{\iota 2\pi \mathbf{k}\cdot\mathbf{a}_\ell} H(\mathbf{x}), \ \ell = 1, 2, 3. \tag{3}$$

Here, $2\pi\mathbf{k}$ is the Bloch wave vector in the first Brillouin zone and $\mathbf{a}_\ell$'s are the lattice translation vectors that span the primitive cell which extends periodically to form the magnetoelectric materials. Figure 1 shows two types of lattice translation vectors that are of particular interest. The first type is the simple cubic (SC) lattice, whose lattice translation vectors are

$$\mathbf{a}_1 = a[1, 0, 0]^\top, \ \mathbf{a}_2 = a\,[0, 1, 0]^\top, \ \mathbf{a}_3 = a\,[0, 0, 1]^\top, \tag{4}$$

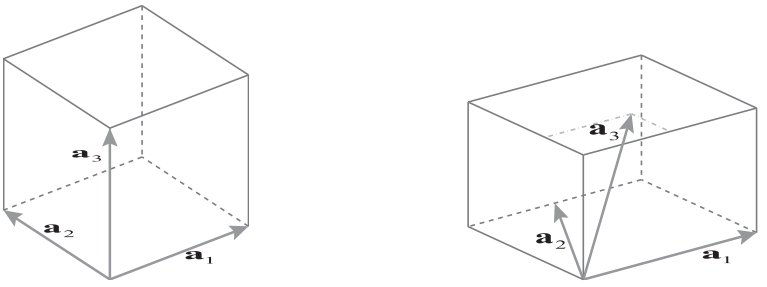

(a) (b)

Figure 1: The translation vectors of (a) simple cubic and (b) face centered cubic lattice.

where a is the lattice constant. The second type is the face centered cubic (FCC) lattice, whose lattice translation vectors are

$$\mathbf{a}_1 = \frac{a}{\sqrt{2}}[1,0,0]^\top,\ \mathbf{a}_2 = \frac{a}{\sqrt{2}}[\frac{1}{2},\frac{\sqrt{3}}{2},0]^\top,\ \mathbf{a}_3 = \frac{a}{\sqrt{2}}[\frac{1}{2},\frac{1}{2\sqrt{3}},\sqrt{\frac{2}{3}}]^\top. \tag{5}$$

Physics breakthroughs and engineering innovations of magnetoelectric metamaterials heavily rely on numerical simulations of the Maxwell equations [6, 12, 13, 21]. Yee's discretization scheme [24] is one of the essential tools among various numerical methods. Solving the eigenvalue problems arising the 3D photonic crystals, dispersive metallic materials and complex media are challenging. Using Yee's scheme and the techniques of matrix analysis, novel numerical methods are proposed in [2, 7, 8, 9, 10, 11] to tackle these challenges and solve these eigenvalue problems efficiently. The key of these proposed methods are the singular value decomposition and eigendecomposition of the discrete single curl and double curl operators, respectively, and the FFT-based matrix-vector multiplications. Despite of the wide use of Yee's scheme, the discrete counterparts of the continuous differential operators and the related properties have not been documented systematically to the best of our knowledge. This article fills the gap by deriving the discrete differential operators in Maxwell's equation and proving several identities from using matrix representations. We also demonstrate how these matrix representations inspire the development of numerical schemes to simulate the magnetoelectric materials.

Throughout this paper, we denote the transpose and the conjugate transpose of a matrix by the superscript $\top$ and $*$, respectively. $\otimes$ is the Kronecker

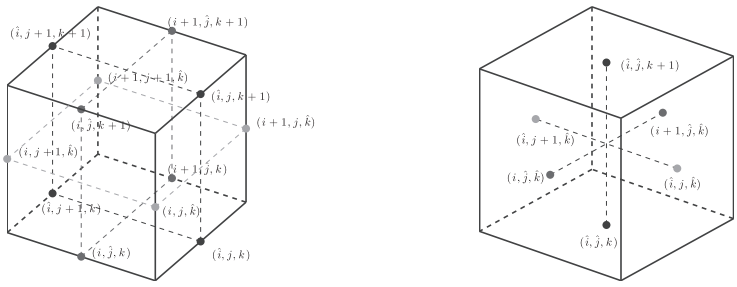

Figure 2: The grid points are located on the (a) edges and (b) faces of primitive cell in Yee's scheme. The figure also shows the corresponding indices.

product. We denote the imaginary number $\sqrt{-1}$ by ι and the identity matrix of order n by I_n. The $\mathrm{vec}(\cdot)$ is the operator that vectorizes a matrix by stacking the columns of the matrix. $\Phi \succ 0$ means that Φ is Hermitian and positive definite.

This paper is outlined as follow. We first derive the explicit matrix representations of the single curl operators in Section 2. Based on these matrix representations, we discuss the eigenvalue problem in different material settings. The discretizations of $\nabla \cdot (\nabla \times) = 0$ and $\nabla \times \nabla = 0$ tell us that the kernel of the eigenvalue problem is huge. We assert the divergence free conditions hold for the null-space free eigenvalue problems in Section 3. Discretizations of operators $\nabla(\nabla\cdot)$ and ∇^2 are derived and some of their properties are verified in Section 4. An efficient preconditioner on the basis of this property is developed in solving the eigenvalue problems arising metallic photonic crystals. Numerical results are presented to demonstrate the efficiency of the proposed methods in Section 5. Finally, we conclude this paper in Section 6.

2. Resulting eigenvalue problems

In Yee's scheme [24], Eqs. (1a) and (1b) are discretized at the centers of cell faces and edges, respectively, with the following notations.

Let δ_x, δ_y, and δ_z denote the grid length along the x, y, and z axial directions, respectively. Let n_1, n_2, and n_3 be the numbers of grid points in x, y, and z axial directions, respectively, and $n = n_1 n_2 n_3$. The approximate function values due to the first order central finite differences are represented

by the grid points indexed by i, j, and k and the "half grid points" indexed by $\hat{i} = i + \frac{1}{2}$, $\hat{j} = j + \frac{1}{2}$, and $\hat{k} = k + \frac{1}{2}$. For simplicity, we represent an arbitrary point $(r\delta_x, s\delta_y, t\delta_z)$ in the computational domain by $\mathbf{x}(r, s, t)$, where $r, s, t \in \mathbb{R}$. That is,

$$\mathbf{x}(r, s, t) = (r\delta_x, s\delta_y, t\delta_z). \tag{6}$$

We further introduce $F(r, s, t)$ to denote the approximate value of function F at the point $\mathbf{x}(r, s, t)$. Next, by using the vectorization function of a matrix $F_\ell \in \mathbb{C}^{m_1 \times m_2 \times m_3}$, for $\ell = 1, 2, 3$,

$$\operatorname{vec}(F_\ell) = \begin{bmatrix} \operatorname{vec}(F_\ell(1:m_1, 1:m_2, 1)) \\ \operatorname{vec}(F_\ell(1:m_1, 1:m_2, 2)) \\ \vdots \\ \operatorname{vec}(F_\ell(1:m_1, 1:m_2, m_3)) \end{bmatrix},$$

we define

$$\mathbf{f} = \begin{bmatrix} \mathbf{f}_1^\top & \mathbf{f}_2^\top & \mathbf{f}_3^\top \end{bmatrix}^\top \in \mathbb{C}^{3m_1m_2m_3}$$

with $\mathbf{f}_\ell = \operatorname{vec}(F_\ell)$, for $\ell = 1, 2, 3$.

Using the Yee's scheme, discretization of $\nabla \times E = \iota\omega B$ by taking central finite differences at the central face points $\mathbf{x}(i, \hat{j}, \hat{k})$, $\mathbf{x}(\hat{i}, j, \hat{k})$, and $\mathbf{x}(\hat{i}, \hat{j}, k)$ leads to the matrix representation

$$C\mathbf{e} = \iota\omega\mathbf{b}, \tag{7}$$

where

$$C = \begin{bmatrix} 0 & -C_3 & C_2 \\ C_3 & 0 & -C_1 \\ -C_2 & C_1 & 0 \end{bmatrix} \tag{8}$$

and

$$C_1 = I_{n_2n_3} \otimes \frac{K_1 - I_{n_1}}{\delta_x},\ C_2 = I_{n_3} \otimes \frac{K_2 - I_{n_2}}{\delta_y} \otimes I_{n_1},\ C_3 = \frac{K_3 - I_{n_3}}{\delta_z} \otimes I_{n_2n_1}, \tag{9}$$

with

$$K_i = \begin{bmatrix} 0 & I_{n_i-1} \\ e^{\iota 2\pi \mathbf{k}\cdot\mathbf{a}_i} & 0 \end{bmatrix},\ i = 1, 2, 3$$

for SC lattice; while

$$C_1 = I_{n_2 n_3} \otimes \frac{K_1 - I_{n_1}}{\delta_x}, \quad C_2 = I_{n_3} \otimes \frac{K_2 - I_{n_1 n_2}}{\delta_y}, \quad C_3 = \frac{K_3 - I_n}{\delta_z}, \tag{10}$$

with

$$K_1 = \begin{bmatrix} 0 & I_{n_1-1} \\ e^{\iota 2\pi \mathbf{k}\cdot\mathbf{a}_1} & 0 \end{bmatrix},$$
$$K_2 = \begin{bmatrix} 0 & I_{(n_2-1)n_1} \\ e^{\iota 2\pi \mathbf{k}\cdot\mathbf{a}_2} J_2 & 0 \end{bmatrix}, \qquad J_2 = \begin{bmatrix} 0 & e^{-\iota 2\pi \mathbf{k}\cdot\mathbf{a}_1} I_{n_1/2} \\ I_{n_1/2} & 0 \end{bmatrix},$$
$$K_3 = \begin{bmatrix} 0 & I_{(n_3-1)n_1 n_2} \\ e^{\iota 2\pi \mathbf{k}\cdot\mathbf{a}_3} J_3 & 0 \end{bmatrix}, \quad J_3 = \begin{bmatrix} 0 & e^{-\iota 2\pi \mathbf{k}\cdot\mathbf{a}_2} I_{n_2/3} \otimes I_{n_1} \\ I_{2n_2/3} \otimes J_2 & 0 \end{bmatrix}$$

for FCC lattice (see [2, 8] for details).

Similarly, discretization of $\nabla \times H = -\iota\omega D$ at the central edge points $\mathbf{x}(\hat{i}, j, k)$, $\mathbf{x}(i, \hat{j}, k)$, and $\mathbf{x}(i, j, \hat{k})$ can be represented by

$$C^* \mathbf{h} = -\iota\omega \mathbf{d}. \tag{11}$$

Based on explicit matrix representations above, we can write down the eigenvalue problem in different material settings.

2.1. Photonic crystals

For the photonic crystals (PCs) with $\mu = 1$, we have $\zeta = \xi = 0$. That is,

$$\mathbf{b} = \mathbf{h}, \quad \mathbf{d} = B_\varepsilon \mathbf{e}, \tag{12}$$

where B_ε is a diagonal matrix which is the discrete counterpart of ε, i.e.,

$$B_\varepsilon = \operatorname{diag} \begin{pmatrix} \operatorname{vec}(\varepsilon(\hat{i}, j, k)|_{(i,j,k)\in\mathcal{S}}) \\ \operatorname{vec}(\varepsilon(i, \hat{j}, k)|_{(i,j,k)\in\mathcal{S}}) \\ \operatorname{vec}(\varepsilon(i, j, \hat{k})|_{(i,j,k)\in\mathcal{S}}) \end{pmatrix}$$

with $\mathcal{S} = \{(i, j, k) : i = 0, \ldots, n_1 - 1, j = 0, \ldots, n_2 - 1, k = 0, \ldots, n_3 - 1\}$. By substituting (7) with (12) into (11), discretizations of (1a) and (1b) become a generalized eigenvalue problem (GEP)

$$A\mathbf{e} = \lambda B_\varepsilon \mathbf{e}, \quad \lambda = \omega^2, \tag{13a}$$

where

$$A = C^*C. \tag{13b}$$

2.2. Complex media

For the complex media, (2) can be rewritten as

$$\begin{bmatrix} \mathbf{b} \\ \mathbf{d} \end{bmatrix} = \begin{bmatrix} D_\zeta & B_\mu \\ -B_\varepsilon & -D_\xi \end{bmatrix} \begin{bmatrix} \mathbf{e} \\ \mathbf{h} \end{bmatrix} \equiv C_{\varepsilon,\mu,\xi,\zeta} \begin{bmatrix} \mathbf{e} \\ \mathbf{h} \end{bmatrix}, \tag{14}$$

where B_μ, D_ζ and D_ξ are the discrete counterparts of μ, ζ and ξ, respectively. Combining the results in (7), (11) and (14), discretizations of (1a) and (1b) becomes a GEP

$$\begin{bmatrix} C & 0 \\ 0 & C^* \end{bmatrix} \begin{bmatrix} \mathbf{e} \\ \mathbf{h} \end{bmatrix} = \iota\omega C_{\varepsilon,\mu,\xi,\zeta} \begin{bmatrix} \mathbf{e} \\ \mathbf{h} \end{bmatrix}. \tag{15}$$

2.3. Huge kernel of eigenvalue problems

The following theorem claims that C_1, C_2 and C_3 are normal and commute with each other, which implies that they can be diagonalized by a common unitary matrix.

Theorem 1 ([2, 8]). *For C_1, C_2 and C_3 defined in* (10)*, it holds that*

$$C_i^* C_j = C_j C_i^* \quad \text{and} \quad C_i C_j = C_j C_i, \quad \text{for } i, j = 1, 2, 3.$$

Furthermore, there exists unitary matrix T such that

$$C_1 T = T\Lambda_1, \quad C_2 T = T\Lambda_2, \quad C_3 T = T\Lambda_3 \tag{16}$$

with diagonal Λ_1, Λ_2 and Λ_3.

In fact, for SC lattice [2], the unitary matrix T in (16) is

$$T = \frac{1}{\sqrt{n}} \left(D_{\mathbf{a}_3,n_3} \otimes D_{\mathbf{a}_2,n_2} \otimes D_{\mathbf{a}_1,n_1} \right) \left(U_{n_3} \otimes U_{n_2} \otimes U_{n_1} \right), \tag{17}$$

where $D_{\mathbf{a}_1,n_1}$, $D_{\mathbf{a}_2,n_2}$, $D_{\mathbf{a}_3,n_3}$ are diagonal, and

$$U_m \equiv \begin{bmatrix} \mathbf{u}_{m,1} & \cdots & \mathbf{u}_{m,m} \end{bmatrix} = \begin{bmatrix} 1 & 1 & \cdots & 1 \\ e^{\theta_{m,1}} & e^{\theta_{m,2}} & \cdots & 1 \\ \vdots & \vdots & & \vdots \\ e^{(m-1)\theta_{m,1}} & e^{(m-1)\theta_{m,2}} & \cdots & 1 \end{bmatrix} \in \mathbb{C}^{m \times m}$$

with $\theta_{m,k} = \frac{\iota 2\pi k}{m}$. For FCC lattice [8],

$$T = \frac{1}{\sqrt{n}} \begin{bmatrix} T_1 & T_2 & \cdots & T_{n_1} \end{bmatrix} \in \mathbb{C}^{n\times n} \tag{18a}$$

where $T_i = \begin{bmatrix} T_{i,1} & T_{i,2} & \cdots & T_{i,n_2} \end{bmatrix} \in \mathbb{C}^{n\times(n_2 n_3)}$ and

$$T_{i,j} = (D_{\hat{\mathbf{a}}_3,i,j} U_{n_3}) \otimes (D_{\hat{\mathbf{a}}_2,i} \mathbf{u}_{n_2,j}) \otimes (D_{\mathbf{a}_1} \mathbf{u}_{n_1,i}) \tag{18b}$$

for $i = 1, \cdots, n_1$, $j = 1, \cdots, n_2$ with diagonal matrices $D_{\mathbf{a}_1}$, $D_{\hat{\mathbf{a}}_2,i}$ and $D_{\hat{\mathbf{a}}_3,i,j}$.

Based on (17), 3D backward and forward fast Fourier transformations (FFTs) can be applied to compute the matrix-vector products $T\mathbf{p}$ and $T^*\mathbf{q}$, respectively, without explicitly forming matrix T. Moreover, for the matrix T in (18), efficient algorithms with 1D backward and forward FFTs have been proposed in [8] to significantly reduce the cost for computing $T\mathbf{p}$ and $T^*\mathbf{q}$, respectively.

As the result in Theorem 1, the singular value decomposition (SVD) of C can be derived along the way in [2], which is shown in Theorem 2.

Theorem 2 ([2])**.** *There exists unitary matrices*

$$Q \equiv \begin{bmatrix} Q_r & Q_0 \end{bmatrix} = (I_3 \otimes T) \left[\begin{array}{cc|c} \Pi_1 & \Pi_2 & \Pi_0 \end{array}\right], \tag{19a}$$

$$P \equiv \begin{bmatrix} P_r & P_0 \end{bmatrix} = (I_3 \otimes T) \left[\begin{array}{cc|c} -\overline{\Pi_2} & \overline{\Pi_1} & \overline{\Pi_0} \end{array}\right], \tag{19b}$$

with $\Pi_j = \begin{bmatrix} \Pi_{j,1}^* & \Pi_{j,2}^* & \Pi_{j,3}^* \end{bmatrix}^*$ *and* $\Pi_{j,k}$ *being diagonal,* $j = 0, 1, 2$, $k = 1, 2, 3$, *such that*

$$C = P \operatorname{diag}\left(\Lambda_q^{1/2}, \Lambda_q^{1/2}, 0\right) Q^* = P_r \Sigma_r Q_r^*, \tag{20a}$$

where

$$\Lambda_q = \Lambda_1^*\Lambda_1 + \Lambda_2^*\Lambda_2 + \Lambda_3^*\Lambda_3,\ \Sigma_r = \operatorname{diag}\left(\Lambda_q^{1/2}, \Lambda_q^{1/2}\right). \tag{20b}$$

From (20a), we know that the nullity of C is equal to n. This result is derived from the viewpoint of matrix analysis, and can also be derived from the discrete version of $\nabla\cdot(\nabla\times) = 0$ and $\nabla\times\nabla = 0$. Let the discrete operator $\nabla_h\times^*$ denote the discretization of curl operator in $\nabla \times H$ at the centers of cell edges and $\nabla_{h,\mathbf{e}}\cdot$ denote the discretization of the divergence operator in $\nabla \cdot E$ at the vertices using Yee's scheme. By a straightforward calculation, we have the identity

$$\nabla_{h,\mathbf{e}} \cdot (\nabla_h \times^*) = 0. \tag{21}$$

From (11), $C^*\mathbf{h}$ is the matrix representation of $\nabla_h \times^* \mathbf{h}$ at the centers of cell edges. On the other hand, the discretization $\nabla_{h,\mathbf{e}} \cdot \mathbf{e}$ can be represented by $-N_c^*\mathbf{e}$, where

$$N_c = \begin{bmatrix} C_1^\top & C_2^\top & C_3^\top \end{bmatrix}^\top. \tag{22}$$

Based on these two facts, Eq. (21) further suggests that

$$N_c^* C^* = 0. \tag{23}$$

By taking the conjugate transpose of (23), we have

$$C N_c = 0. \tag{24}$$

Eqs. (23) and (24) imply that the kernels of the eigenvalue problems in (13) and (15) are huge.

The result in (24) can be also derived from the discretization of $\nabla \times \nabla = 0$. Denoting $G = \nabla F$, we discretize $\partial_x F$, $\partial_y F$ and $\partial_z F$ at $\mathbf{x}(\hat{i}, j, k)$, $\mathbf{x}(i, \hat{j}, k)$ and $\mathbf{x}(i, j, \hat{k})$, respectively, which leads to the matrix form

$$\mathbf{g} = N_c \mathbf{f}. \tag{25a}$$

By a straightforward calculation, we also have the identity

$$\nabla_h \times \nabla_h \equiv 0. \tag{25b}$$

Moreover, it is known that C is the matrix representation of $\nabla_h \times$, therefore, (25) also implies (24).

A short summary of above discretizations is listed in Table 1.

3. Eigenvalue problems incorporated with divergence free conditions

In this section we will show that, under certain assumption, the divergence free conditions corresponding to the photonic crystals and complex media in Yee's scheme are automatically satisfied.

3.1. $\nabla \cdot (\varepsilon E) = 0$ in photonic crystals

We consider the GEP (13) of photonic crystals in terms of the electric field E. In this case, there is only one divergence free condition $\nabla \cdot (\varepsilon E) = 0$. From

Table 1: Explicit matrix representations and discretization points of differential operators and operations within the Maxwell equations

Cont. operator	$\nabla \times H$	$\nabla \times E$	$\nabla \cdot E$	∇F
Disc. operator	$\nabla_h \times^*$	$\nabla_h \times$	$\nabla_{h,\mathbf{e}} \cdot$	∇_h
Matrix form	$C^*\mathbf{h}$	$C\mathbf{e}$	$-N_c^*\mathbf{e}$	$N_c\mathbf{f}$
Discretized pts	$\mathbf{x}(\hat{i}, j, k)$	$\mathbf{x}(i, \hat{j}, \hat{k})$	$\mathbf{x}(i, j, k)$	$\mathbf{x}(\hat{i}, j, k)$
	$\mathbf{x}(i, \hat{j}, k)$	$\mathbf{x}(\hat{i}, j, \hat{k})$		$\mathbf{x}(i, \hat{j}, k)$
	$\mathbf{x}(i, j, \hat{k})$	$\mathbf{x}(\hat{i}, \hat{j}, k)$		$\mathbf{x}(i, j, \hat{k})$

	Photonic crystal	Complex media
Cont. operator	$\nabla \times \nabla \times E = \omega^2 \varepsilon E$	$\nabla \times E = \iota\omega(\mu H + \zeta E)$ $\nabla \times H = -\iota\omega(\varepsilon E + \xi H)$
Eigenvalue prob.	$C^*C\mathbf{e} = \lambda B_\varepsilon \mathbf{e}$	(15)

Cont. operator	$\nabla \cdot (\nabla \times) = 0$	$\nabla \times \nabla = 0$
Discrete operator	$\nabla_{h,\mathbf{e}} \cdot (\nabla_h \times^*) = 0$	$\nabla_h \times (\nabla_h) = 0$
Matrix form	$N_c^* C^* = 0$	$CN_c = 0$
Indication	$\nabla_h \times$ has large kernel in Yee's scheme	

Section 2.3, we know that the discretization $\nabla_{h,\mathbf{e}} \cdot \mathbf{e}$ can be represented by $-N_c^*\mathbf{e}$, which suggests that the discrete version of the divergence free constraint $\nabla \cdot (\varepsilon E) = 0$ can be written as

$$N_c^* (B_\varepsilon \mathbf{e}) = 0. \tag{26}$$

That is, $B_\varepsilon \mathbf{e}$ is orthogonal to the subspace $\mathcal{N}_c$ spanned by N_c. From (24), $\mathcal{N}_c$ is a null-space of $A = C^*C$. Since A is Hermitian positive semidefinite, the invariant subspace $\mathcal{R}_A$ of A corresponding to all positive eigenvalues is orthogonal to $\mathcal{N}_c$. Therefore if we take $B_\varepsilon \mathbf{e} \in \mathcal{R}_A$, then the divergence free constraint in (26) is automatically satisfied.

By Theorem 2, we have the eigendecomposition of A in (13b) as

$$A = Q \mathrm{diag}\left(0, \Sigma_r^2\right) Q^* = Q_r \Sigma_r^2 Q_r^*. \tag{27}$$

Applying (27), the huge null-space of the GEP (13) can be completely deflated as shown below.

Theorem 3 ([8, 9])**.** *Let Q_r and Σ_r be defined in Theorem 2. Then we have*

$$span\left\{B_\varepsilon^{-1} Q_r \Sigma_r\right\} = \{\mathbf{e} \mid A\mathbf{e} = \lambda B_\varepsilon \mathbf{e},\ \lambda > 0\} \tag{28}$$

and the GEP (13) *can be transformed to a null-space free standard eigenvalue problem (NFSEP)*

$$K_r\mathbf{y} \equiv \left(\Sigma_r Q_r^* B_\varepsilon^{-1} Q_r \Sigma_r\right)\mathbf{y} = \lambda\mathbf{y} \tag{29}$$

with

$$\mathbf{e} = B_\varepsilon^{-1} Q_r \Sigma_r \mathbf{y} \tag{30}$$

being eigenvector of (13)*. Both of the GEP and the corresponding NFSEP have the same positive eigenvalues, while the zero eigenvalues of the GEP are deflated.*

Now, we show the divergence free constraint (26) is automatically satisfied if the null-space free method in Theorem 3 is applied to solve the GEP (13).

Theorem 4. *Let* $\mathbf{y}$ *be an eigenvector of* (29) *and* $\mathbf{e}$ *be defined in* (30)*. Then* $\mathbf{e}$ *automatically satisfies the divergence free constraint* (26)*.*

Proof. Using (30), it holds that

$$B_\varepsilon \mathbf{e} = Q_r \Sigma_r \mathbf{y}.$$

From (24) and (27), the columns of N_c and Q_r, respectively, span the invariant subspaces of the Hermitian matrix A corresponding to zero and nonzero eigenvalues. This implies that

$$N_c^*(B_\varepsilon \mathbf{e}) = N_c^* Q_r \Sigma_r \mathbf{y} = 0.$$

This means that such eigenvector $\mathbf{e}$ automatically satisfies (26). □

3.2. $\nabla \cdot B = 0$ and $\nabla \cdot D = 0$ in complex media

We consider the case of complex media in this section. From the discretization of the divergence operator in $\nabla \cdot B$, denoted by $\nabla_{h,\mathbf{b}}\cdot$, at the cubic central points $\mathbf{x}(\hat{i}, \hat{j}, \hat{k})$, we can see that the discrete counterpart of $\nabla \cdot B$ can be represented as $C_1\mathbf{b}_1 + C_2\mathbf{b}_2 + C_3\mathbf{b}_3$. In other words, the discrete version of the divergence free constraint $\nabla \cdot B = 0$ is

$$C_1\mathbf{b}_1 + C_2\mathbf{b}_2 + C_3\mathbf{b}_3 = 0. \tag{31}$$

Similarly, the discretization of $\nabla \cdot D$ at the vertices suggests that the discrete version of the divergence free constraint $\nabla \cdot D = 0$ is

$$C_1^* \mathbf{d}_1 + C_2^* \mathbf{d}_2 + C_3^* \mathbf{d}_3 = 0. \tag{32}$$

Define

$$N_l^* = \begin{bmatrix} C_1 & C_2 & C_3 & 0 & 0 & 0 \\ 0 & 0 & 0 & C_1^* & C_2^* & C_3^* \end{bmatrix}.$$

From (14), (31) and (32), the divergence free constraints $\nabla \cdot B = 0$ and $\nabla \cdot D = 0$ result in the constraint

$$N_l^* \begin{bmatrix} \mathbf{b} \\ \mathbf{d} \end{bmatrix} = 0 \;\Rightarrow\; N_l^* C_{\varepsilon,\mu,\xi,\zeta} \begin{bmatrix} \mathbf{e} \\ \mathbf{h} \end{bmatrix} = 0. \tag{33}$$

On the other hand, by the definition of C in (8) and the commute property in Theorem 1, it holds that

$$N_l^* \begin{bmatrix} C & 0 \\ 0 & C^* \end{bmatrix} = 0. \tag{34}$$

That is, $\mathrm{span}\{N_l\}$ is the left null-space of $\mathrm{diag}(C, C^*)$. Combining the results in (33) and (34), we know that if $[\mathbf{b}^\top, \mathbf{d}^\top]^\top$ belongs to the subspace $\mathcal{S}_l$ generated by the left singular vectors corresponding to all positive singular values of $\mathrm{diag}(C, C^*)$, then the discrete divergence free constraints in (33) are automatically satisfied.

In [2], a null-space free method with applying SVD of C in (20a) has been proposed to solve the GEP (15).

Theorem 5 ([2]). *If $C_{\varepsilon,\mu,\xi,\zeta}$ in* (15) *is nonsingular, then*

$$\mathrm{span}\left\{ C_{\varepsilon,\mu,\xi,\zeta}^{-1} \mathrm{diag}\left(P_r \Sigma_r^{\frac{1}{2}}, Q_r \Sigma_r^{\frac{1}{2}} \right) \right\}$$

is an invariant subspace of (15) *corresponding to all nonzero eigenvalues. Furthermore, the GEP in* (15) *can be reduced to a $4n \times 4n$ null-space free GEP (NFGEP)*

$$\widehat{A}_r \mathbf{y}_r = \omega \left(\iota \begin{bmatrix} 0 & \Sigma_r^{-1} \\ -\Sigma_r^{-1} & 0 \end{bmatrix} \right) \mathbf{y}_r \equiv \omega \widehat{B}_r \mathbf{y}_r, \tag{35}$$

and

$$\begin{bmatrix} \mathbf{e}^\top & \mathbf{h}^\top \end{bmatrix}^\top = C_{\varepsilon,\mu,\xi,\zeta}^{-1} \mathrm{diag}\left(P_r, Q_r \right) \mathbf{y}_r \tag{36}$$

is the corresponding eigenvector of (15)*, where*

(37)
$$\widehat{A}_r \equiv \operatorname{diag}(P_r^*, Q_r^*) \begin{bmatrix} B_\mu^{-1} D_\zeta & -I_{3n} \\ I_{3n} & 0 \end{bmatrix} \begin{bmatrix} \Phi^{-1} & 0 \\ 0 & B_\mu^{-1} \end{bmatrix} \begin{bmatrix} D_\xi B_\mu^{-1} & I_{3n} \\ -I_{3n} & 0 \end{bmatrix} \operatorname{diag}(P_r, Q_r)$$

with $\Phi \equiv B_\varepsilon - D_\xi B_\mu^{-1} D_\zeta$.

Similarly, the divergence free constraints (33) is automatically satisfied if the null-space free method is applied to solve (15), as shown in Theorem 6.

Theorem 6. *Let* $\mathbf{y}_r$ *be an eigenvector of* (35) *and* $[\mathbf{e}^\top, \mathbf{h}^\top]^\top$ *be defined in* (36)*. Then* $[\mathbf{e}^\top, \mathbf{h}^\top]^\top$ *automatically satisfies the divergence free condition* (33)*.*

Proof. Using (36), we have

$$C_{\varepsilon,\mu,\xi,\zeta} \begin{bmatrix} \mathbf{e}^\top & \mathbf{h}^\top \end{bmatrix}^\top = \operatorname{diag}(P_r, Q_r)\, \mathbf{y}_r.$$

From Theorem 2 and (34), $\operatorname{span}\{N_l\} = \operatorname{span}\{\operatorname{diag}(P_0, Q_0)\}$ and then

$$N_l^* \operatorname{diag}(P_r, Q_r) = 0,$$

which implies that

$$N_l^* C_{\varepsilon,\mu,\xi,\zeta} \begin{bmatrix} \mathbf{e}^\top & \mathbf{h}^\top \end{bmatrix}^\top = N_l^* \operatorname{diag}(P_r, Q_r)\, \mathbf{y}_r = 0.$$

This means that such eigenvector $[\mathbf{e}^\top, \mathbf{h}^\top]^\top$ automatically satisfies (33). □

Furthermore, if we assume that

(38)
$$B_\mu \succ 0,\ \Phi \equiv B_\varepsilon - D_\xi B_\mu^{-1} D_\zeta \succ 0,\ \text{and}\ D_\xi^* = D_\zeta,$$

i.e., B_μ and Φ are Hermitian and positive definite, then A_r is Hermitian and positive definite, which means that all eigenvalues of (15) are real.

A short summary of above divergence free constraints is listed in Table 2.

3.3. Advantages of null-space free eigenvalue problems

To solve the GEPs (13) and (15) is not an easy task due to the following numerical challenge. From (24), we see that the multiplicity of the zero eigenvalue of (13) and (15) is one third of the dimension of the coefficient matrix. As we are interested in finding a few of the smallest positive eigenvalues, the large dimension of the null-space will degrade the computational efficiency of eigensolvers [7, 11]. However, the null-space free eigenvalue problems in (29)

Table 2: Subjects in the derivation regarding the reasons that the divergence free constraints are automatically satisfied in the null-space free eigenvalue problems due to Yee's scheme

Cont. operator	$\nabla \cdot \tilde{E}$	$\nabla \cdot B$	$\nabla \cdot D$
Disc. operator	$\nabla_{h,\mathbf{e}} \cdot$		
Matrix form	$-N_c^* \tilde{\mathbf{e}}$	$[C_1, C_2, C_3]\mathbf{b}$	$-N_c^* \mathbf{d}$
Discretized pts	$\mathbf{x}(i,j,k)$	$\mathbf{x}(\hat{i},\hat{j},\hat{k})$	$\mathbf{x}(i,j,k)$
Div. free	$\nabla \cdot \tilde{E} = 0$	$\nabla \cdot B = 0$, $\nabla \cdot D = 0$	
Matrix form	$N_c^* \tilde{\mathbf{e}} = 0$	$N_l^* [\mathbf{b}^* \ \ \mathbf{d}^*]^* = 0$	
Condition	$\tilde{\mathbf{e}} \equiv B_\varepsilon \mathbf{e} \in \mathcal{R}_A$	$[\mathbf{b}^* \ \ \mathbf{d}^*]^* \equiv C_{\varepsilon,\mu,\xi,\zeta} [\mathbf{e}^* \ \ \mathbf{h}^*]^* \in \mathcal{S}_l$	

	Photonic crystal	Complex media
Eigenvalue prob.	(13)	(15)
Div. free	$\nabla \cdot (\varepsilon E) = 0$	$\nabla \cdot B = 0, \ \nabla \cdot D = 0$
Decomposition	$C^*C = Q_r \Lambda_r Q_r^*$	$C = P_r \Sigma_r Q_r^*$
Subspace	$\mathcal{R}_A = \text{span}\{Q_r\}$	$\mathcal{S}_l = \text{span}\{\text{diag}(P_r, Q_r)\}$
Condition	$\mathbf{e} \in \text{span}\{B_\varepsilon^{-1} Q_r\}$	$[\mathbf{e}^* \ \ \mathbf{h}^*]^* \in \text{span}\{C_{\varepsilon,\mu,\xi,\zeta}^{-1} \text{diag}(P_r, Q_r)\}$
Null-space free	(29)	(35)

and (35) share the same nonzero eigenvalues for (13) and (15), respectively, so that the zero eigenvalues disappear and do not slow down the convergence in solving (29) and (35). Furthermore, in each iteration of solving (29) and (35), we must solve the linear systems of forms

$$Q_r^* B_\varepsilon^{-1} Q_r \mathbf{y} = \mathbf{b}, \tag{39a}$$

$$A_r \mathbf{y} = \mathbf{b}, \tag{39b}$$

respectively, for a given vector $\mathbf{b}$. Because $Q_r^* B_\varepsilon^{-1} Q_r$ and A_r are Hermitian and positive definite, the linear systems in (39) can be solved efficiently by the conjugate gradient (CG) method without any preconditioner. The associated matrix-vector multiplications of the forms $(T^*\mathbf{p}, T\mathbf{q})$ for computing $(P_r^* \hat{\mathbf{p}}_1, Q_r^* \hat{\mathbf{p}}_2)$ and $(P_r \hat{\mathbf{q}}_1, Q_r \hat{\mathbf{q}}_2)$, which are the most costly parts of solving (39), can be computed efficiently by the fast Fourier transformation (FFT) [2, 8].

4. Efficient preconditioner with applying discretizations of $\nabla(\nabla\cdot)$ and ∇^2 for metallic photonic crystals

In Section 4.1, we will derive the matrix representations of the second order differential operators $\nabla(\nabla\cdot)$ and ∇^2 with Yee's scheme, which have some important applications in dispersive metallic photonic crystals. In Section 4.2,

we will show that these matrix representations further inspire us to develop efficient methods for solving the linear systems embedded in the shift-and-invert type eigensolvers with various photonic crystal simulators.

4.1. Discretizations of $\nabla(\nabla\cdot)$ and ∇^2

Here, we let $\nabla_h(\nabla_{h,\mathbf{e}}\cdot E)$ and $\nabla_h^2 E$ denote the discrete version of $\nabla(\nabla\cdot E)$ and $\nabla^2 E$, respectively, with Yee's scheme.

Lemma 7. *Let N_c be defined in* (22)*. The matrix representations of $\nabla_h(\nabla_{h,\mathbf{e}}\cdot E)$ and $\nabla_h^2 E$ are $-N_c N_c^*\mathbf{e}$ and $-I_3\otimes(N_c^* N_c)\,\mathbf{e}$, respectively. Furthermore,*

$$\nabla_h \times^* \nabla_h \times E = \nabla_h(\nabla_{h,\mathbf{e}}\cdot E) - \nabla_h^2 E, \tag{40}$$

which is the discrete counterpart of

$$\nabla\times\nabla\times E = \nabla(\nabla\cdot E) - \nabla^2 E. \tag{41}$$

Proof. From Sections 2.3 and 3.1, the discretization of $G = \nabla F$ and $F = \nabla\cdot E$ at the central edge points and the vertices, respectively, leads to

$$\mathbf{g} = N_c\mathbf{f}, \quad \mathbf{f} = -N_c^*\mathbf{e}, \tag{42}$$

which means that the discretization for $G = \nabla(\nabla\cdot E)$ is of the form $\mathbf{g} = -N_c N_c^*\mathbf{e}$.

In the discretization of ∇^2, we rewrite $\nabla^2 E_1$ as $\nabla\cdot(\nabla E_1)$ and set $F = \nabla E_1$. For the discretizations of $F_1 = \partial_x E_1$, $F_2 = \partial_y E_1$ and $F_3 = \partial_z E_1$ with the quasi-periodic conditions (3) at $\mathbf{x}(i,j,k)$, $\mathbf{x}(\hat{i},\hat{j},k)$ and $\mathbf{x}(\hat{i},j,\hat{k})$, respectively, we have the matrix forms

$$\mathbf{f}_1 = -C_1^*\mathbf{e}_1,\ \mathbf{f}_2 = C_2\mathbf{e}_1,\ \mathbf{f}_3 = C_3\mathbf{e}_1. \tag{43}$$

On the other hand, we discrete $\nabla\cdot F$ at the central edge points $\mathbf{x}(\hat{i},j,k)$ which results in the matrix representation

$$C_1\mathbf{f}_1 - C_2^*\mathbf{f}_2 - C_3^*\mathbf{f}_3. \tag{44}$$

Now, substituting (43) into (44), we obtain the matrix form of the discretization for $\nabla^2 E_1$ as

$$-(C_1C_1^* + C_2^*C_2 + C_3^*C_3)\,\mathbf{e}_1 = -N_c^* N_c\mathbf{e}_1. \tag{45}$$

Similarly, the matrix representations of the discretization of $\nabla^2 E_2$ and $\nabla^2 E_3$ are

$$-N_c^* N_c \mathbf{e}_2 \quad \text{and} \quad -N_c^* N_c \mathbf{e}_3, \tag{46}$$

respectively. Finally, combining (45) and (46), we see that the matrix form of the discretization of $\nabla^2 E$ is $-(I_3 \otimes N_c^* N_c)\,\mathbf{e}$.

On the other hand, the commute property in Theorem 1 implies that

$$C^* C = I_3 \otimes (N_c^* N_c) - N_c N_c^*. \tag{47}$$

It is thus clear that Eq. (47) is the explicit matrix representation of the discretization in (40). □

4.2. Efficient preconditioner to the eigensolvers

For the dispersive metallic photonic crystals [3, 4, 5, 16, 17, 22], Yee's discretization results a rational eigenvalue problem (REP)

$$C^* C \mathbf{e} = \omega^2 B_\varepsilon(\omega) \mathbf{e}, \tag{48}$$

where $B_\varepsilon(\omega)$ is diagonal with diagonal entries being rational functions in variable ω. For the lossless Drude model

$$\varepsilon(\omega) = 1 - \frac{\omega_p^2}{\omega^2}$$

with plasma frequency ω_p, the REP (48) can be reduced to a SEP [10]:

$$\left(C^* C + \omega_p^2 B_d\right) \mathbf{e} = \lambda \mathbf{e}, \quad \lambda = \omega^2, \tag{49}$$

where B_d is a diagonal constant matrix. The most expensive computational task in solving (49) with the Jacobi-Davidson method is a series of linear systems in the form

$$(I - \mathbf{u}\mathbf{u}^*)\,(C^* C + \omega_p^2 B_d - \theta I)\,(I - \mathbf{u}\mathbf{u}^*)\,\mathbf{t} = -\mathbf{r}, \quad \mathbf{t} \perp \mathbf{u} \tag{50}$$

or

$$\left(C^* C + \omega_p^2 B_d - \sigma I\right) \mathbf{t} = \mathbf{b}. \tag{51}$$

Here, $(\theta, \mathbf{u})$ is the current approximate eigenpair of the SEP (49) and $\mathbf{r} = \left(C^* C + \omega_p^2 B_d\right) \mathbf{u} - \theta \mathbf{u}$ is the corresponding residual vector.

As suggested in [7, 10, 9],

$$M = C^*C - \alpha I, \tag{52}$$

where α is the average of all diagonal entries of $(\theta I - \omega_p^2 B_d)$ or $(\sigma I - \omega_p^2 B_d)$, is an efficient preconditioner and Lemma 7 actually suggests an efficient way to solve the preconditioned linear system

$$(C^*C - \alpha I)\mathbf{y} = \mathbf{d}. \tag{53}$$

Theorem 8. *Let* Λ_1, Λ_2, Λ_3 *be defined in* (16) *and* Λ_q *be defined in* (20b). *The preconditioned linear system* (53) *can be transformed as*

$$(I_3 \otimes \Lambda_q - \alpha I)\,\tilde{\mathbf{y}} = \left(I - \alpha^{-1} \begin{bmatrix} \Lambda_1 \\ \Lambda_2 \\ \Lambda_3 \end{bmatrix} \begin{bmatrix} \Lambda_1^* & \Lambda_2^* & \Lambda_3^* \end{bmatrix} \right) (I_3 \otimes T)^*\,\mathbf{d} \tag{54a}$$

and

$$\mathbf{y} = (I_3 \otimes T)\,\tilde{\mathbf{y}}. \tag{54b}$$

Proof. From (47), Eq. (53) can be reformulated into

$$\{I_3 \otimes (N_c^* N_c) - \alpha I\}\,\mathbf{y} = \mathbf{d} + N_c N_c^* \mathbf{y}. \tag{55}$$

Multiplying (53) by $N_c N_c^*$ and considering that $CN_c = 0$, we have

$$N_c N_c^* \mathbf{y} = -\alpha^{-1} N_c N_c^* \mathbf{d}$$

and Eq. (55) becomes

$$\{I_3 \otimes (N_c^* N_c) - \alpha I\}\,\mathbf{y} = \mathbf{d} - \alpha^{-1} N_c N_c^* \mathbf{d}. \tag{56}$$

Applying the eigen-decompositions of C_ℓ's in (16), the solution $\mathbf{y}$ in (56) can be computed by (54). □

A short summary of above discretizations is listed in Table 3.

5. Numerical results

To study the convergence behavior of the linear solvers and the eigensolvers in terms of iteration numbers, we consider the setup described in [1, 9]. The media consists of solid dielectric spheres with a connecting spheroid, as

Table 3: Efficient preconditioner within dispersive metallic PC

Cont. operator	$\nabla \cdot E$	∇F	∇E_1	$\nabla \cdot F$
Disc. operator	$\nabla_{h,\mathbf{e}}\cdot$	∇_h		
Matrix form	$-N_c^*\mathbf{e}$	$N_c\mathbf{f}$	$[-C_1 \;\; C_2^* \;\; C_3^*]^*\,\mathbf{e}_1$	$C_1\mathbf{f}_1 - C_2^*\mathbf{f}_2 - C_3^*\mathbf{f}_3$
Discretized pts	$\mathbf{x}(i,j,k)$	$\mathbf{x}(\hat{i},j,k)$	$\mathbf{x}(i,j,k)$	$\mathbf{x}(\hat{i},j,k)$
		$\mathbf{x}(i,\hat{j},k)$	$\mathbf{x}(\hat{i},\hat{j},k)$	
		$\mathbf{x}(i,j,\hat{k})$	$\mathbf{x}(\hat{i},\hat{j},k)$	
Cont. operator	$\nabla(\nabla \cdot E)$		$\nabla^2 E_1$	$\nabla^2 E$
Matrix form	$-N_cN_c^*\mathbf{e}$		$-(N_c^*N_c)\mathbf{e}_1$	$-[I_3 \otimes (N_c^*N_c)]\mathbf{e}$

Continuous operator	$\nabla \times \nabla \times E = \nabla(\nabla \cdot E) - \nabla^2 E$
Discrete operator	$\nabla_h \times^* \nabla_h \times E = \nabla_h(\nabla_{h,\mathbf{e}} \cdot E) - \nabla_h^2 E$
Matrix form	$C^*C = I_3 \otimes (N_c^*N_c) - N_cN_c^*$
Application	Efficient preconditioner within metallic PC
Preconditioning LS	$(C^*C - \alpha I)\mathbf{y} = \mathbf{d}$
New form	$\{I_3 \otimes (N_c^*N_c) - \alpha I\}\,\mathbf{y} = \mathbf{d} - \alpha^{-1}N_cN_c^*\mathbf{d}$

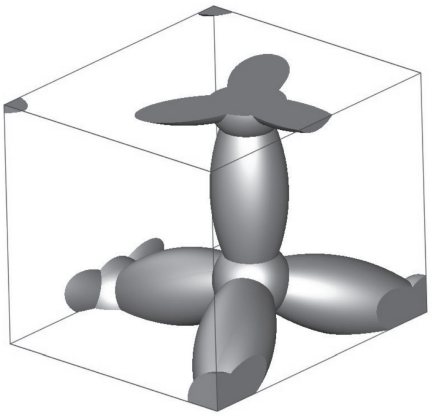

Figure 3: The schema of a face-centered cubic structure in a primitive cell.

shown in Figure 3. r denotes the radius of the spheres and the connecting spheroid has a minor axis of length s. Inside the structure is the dielectric material with permittivity contrast $\varepsilon_i/\varepsilon_o = 13$ for 3D photonic crystals and complex media.

For the implementation, the MATLAB function `eigs` is used to solve the NSFEP (29), NFGEP (35) and SEP (49). `pcg` (without preconditioning) and `bicgstabl` with preconditioner M in (52) are used to solve the linear systems (39) and (51), respectively. `fft` and `ifft` are applied to compute the matrix-vector products $T^*\mathbf{p}$ and $T\mathbf{q}$, respectively. All computations are

Table 4: Dimensions of the matrices for $n_1 = 96$ and $n_1 = 198$, where $n_1 = n_2 = n_3$

	matrix	n_1	$n_1 = 96$	$n_1 = 198$
dimension	K_r	$2n_1^3$	1,769,472	15,524,784
	A_r	$4n_1^3$	3,538,944	31,049,568
	C	$3n_1^3$	2,654,208	23,287,176

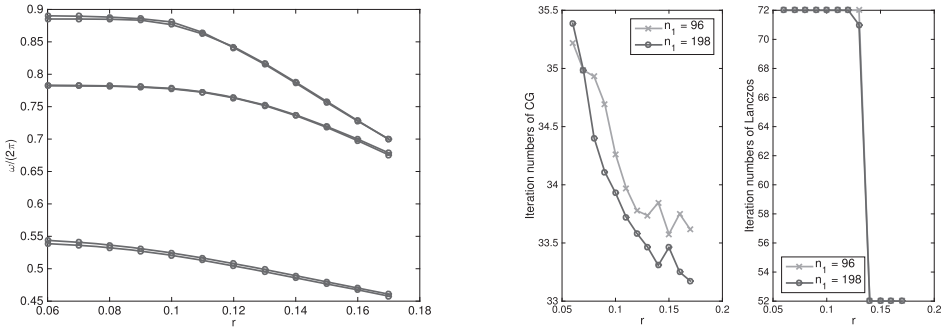

(a) Band structure (b) Iteration numbers

Figure 4: The band structure (frequency curves) for the 3D photonic crystals, the average of iteration number of `pcg`, and the iteration numbers of `eigs` with various radius r of the sphere.

performed in MATLAB 2014b. The matrix sizes of K_r, A_r and C in (29), (35) and (49) are listed in Table 4.

For the hardware configuration, we use a HP workstation equipped with two Intel Quad-Core Xeon E5-2643 3.33GHz CPUs, 96 GB of main memory, and RedHat Enterprise Linux 6 operating system.

- **Photonic crystals.** The minor axis length s of the connecting spheroid is set to be 0.11. Figure 4(a) shows the band structure with various radius r of sphere and $n_1 = n_2 = n_3 = 96$.
  Figure 4(b) shows that the average iteration numbers for solving the linear system (39a) within the invert Lanczos method and the iteration numbers of the invert Lanczos method with $n_1 = 96$ and $n_1 = 198$.
- **Complex media.** We consider the pseudochiral media and assert that the corresponding magnetoelectric coupling matrices D_ξ and D_ζ satisfy the assumptions given in (38). We can therefore solve the NFGEP in

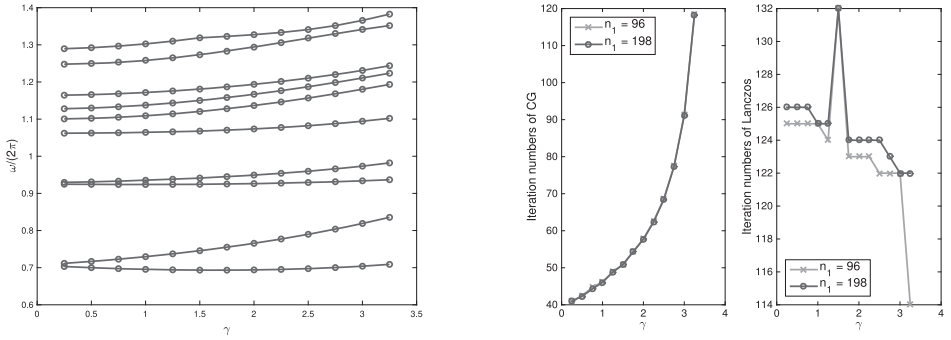

(a) Band structure (b) Iteration numbers

Figure 5: The band structure (frequency curves) of 3D pseudochiral media, the average of iteration number of `pcg`, and the iteration numbers of `eigs` with various chirality parameter γ.

(35) using the Lanczos method. Specifically, D_ξ and D_ζ are

$$D_\xi = \begin{bmatrix} 0 & 0 & \iota\gamma\tilde{I}_1 \\ 0 & 0 & 0 \\ \iota\gamma\tilde{I}_2 & 0 & 0 \end{bmatrix} \text{ and } D_\zeta = \begin{bmatrix} 0 & 0 & -\iota\gamma\tilde{I}_2 \\ 0 & 0 & 0 \\ -\iota\gamma\tilde{I}_1 & 0 & 0 \end{bmatrix}. \tag{57}$$

Here, γ is the chirality parameter, and $\tilde{I}_1, \tilde{I}_2 \in \mathbb{R}^{n\times n}$ are diagonal matrices whose entries are 0 (outside of the medium) or 1 (within the medium) depending on the corresponding locations of grid points. The permeability μ is usually taken as I_3, so the matrix B_μ in (14) is the identity matrix. Therefore, Φ in (38) is also diagonal and its diagonal entries are positive if $\gamma \in (0, \sqrt{\varepsilon_i})$. The radius of the spheres r and the minor axis length s of the connecting spheroid are set to be $r = 0.12$ and $s = 0.11$, respectively. Figure 5(a) shows the band structure with various chirality parameter γ and $n_1 = n_2 = n_3 = 96$.
Figure 5(b) shows that the average iteration numbers for solving the linear system (39b) within the invert Lanczos method and the iteration numbers of the invert Lanczos method with $n_1 = 96$ and $n_1 = 198$.

- **Metallic photonic crystals.** We take the plasma frequency $\omega_p = 10\pi$ and ε_o of the non-dispersive material to be equal to 1. The minor axis length s of the connecting spheroid is set to be 0.11. Figure 6(a) shows the band structure with various radius r of sphere and $n_1 = n_2 = n_3 = 96$.

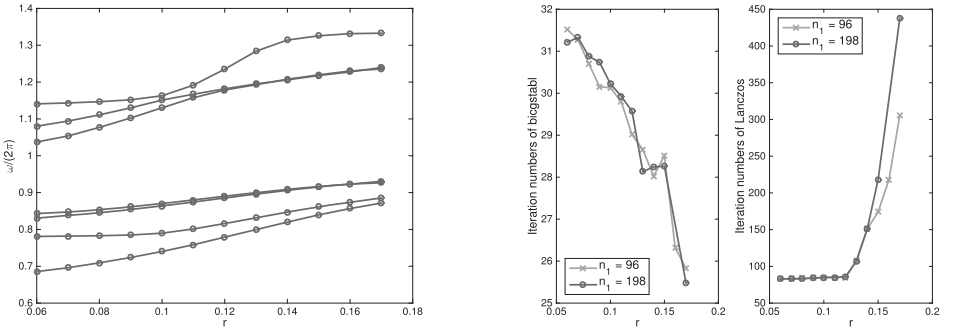

(a) Band structure (b) Iteration numbers

Figure 6: The band structure (frequency curves) for the 3D dispersive metallic photonic crystals, the average of iteration number of `bicgstbl`, and the iteration numbers of `eigs` with various radius r of the sphere.

Figure 6(b) shows that the average iteration numbers for solving the linear system (51) within the shift-and-invert Lanczos method and the iteration numbers of the shift-and-invert Lanczos method with $n_1 = 96$ and $n_1 = 198$.

Based on Figures 4(b), 5(b), and 6(b), we highlight the performance of the proposed method.

- **The iteration numbers are very small.** Figures 4(b), 5(b), and 6(b) show the iteration numbers of the Lanczos method for solving NSFEP in (29), NFGEP in (35) and SEP in (49) with different parameter combinations. In all cases, the iteration numbers are rather small in Table 4. Because huge null-spaces have been deflated in (29) and (35), the iteration numbers in Figures 4(b) and 5(b), in average, are only 65 and 125 even the matrix size is as large as 15.5 million and 31.0 million, respectively.
- **The linear systems in the form of** (39) **are well-conditioned for the tested r's and γ's.** Here we take a close look at the behavior of `pcg` used to solve the linear systems (39a) and (39b) with various r's and γ's, respectively. As shown in Figures 4(b) and 5(b), the (average) iteration numbers of `pcg` for solving (39a) and (39b) in the tested eigenvalue problems increase from 33 to 36 and from 40 to 120, respectively. The behavior in Figure 4(b) is due to well-conditioned coefficient matrices in (39a). The associated condition number is independent on the matrix size and the radius r of spheres so that the

CG method takes only around 34 iterations consistently for all of the tested problems even the matrix size is as large as 15.5 million. The behavior in Figure 5(b) is in line with the increase in the condition number of the coefficient matrix A_r in (39b) as γ varies from 0.25 to 3.25 (A_r is singular as $\gamma = \sqrt{\varepsilon_i} \approx 3.61$). For problems as large as 31.0 million, these small iteration numbers suggest that the coefficient matrix A_r is quite well-conditioned.

- **The preconditioner M in (52) is an efficient preconditioner in solving linear system (51).** Figure 6(b) shows that `bicgstbl` with preconditioner M takes around 29 iterations for convergence. We would like to emphasize that, for the linear system (51) with dimensions as large as 23.3 million, these results suggest that the preconditioning schemes proposed in Section 4.2 for (52) are indeed efficient.

6. Conclusion

Yee's scheme is one of the essential tools to solve the Maxwell's equations. Our goal is to deepen the understanding of such scheme from the viewpoint of matrix computation. First, in Section 2.3, we prove the discrete counterparts of the continuous divergence of curl $\nabla\cdot\nabla\times = 0$ and the continuous curl of gradient identify $\nabla \times \nabla\phi = 0$ in Eq. (21) and Eq. (25b), respectively. The result shows that there is a large kernel of the discrete curl operator $\nabla_h\times$. For the eigenvalue problems (13) and (15) formed by the curl operator, such a large kernel can deteriorate the convergence of the eigenvalue solvers.

Second, in Sections 3.1 and 3.2, we assert the discrete counterpart of the continuous divergence free conditions $\nabla\cdot(\varepsilon E) = 0$ and $\nabla\cdot B = 0, \nabla\cdot D = 0$ in Eqs. (26) and (33), respectively. Eqs. (26) and (33) lead to the fact that if the vector belongs to the invariant subspaces corresponding to nonzero eigenvalues, then the divergence free conditions automatically hold. Nullspace-free methods developed in [2, 8] provide these invariant subspaces and reduce the original eigenvalue problems (13) and (15) into smaller eigenvalue problems (29) and (35), respectively, without any zero eigenvalues. The divergence free conditions in (26) and (33) automatically hold and the issue is overcome of slowing downg the convergence of eigensolvers for the large kernel.

Third, in Section 4.1, we prove the discrete counterpart of the continuous curl of curl identify $\nabla \times \nabla \times E = \nabla(\nabla \cdot E) - \nabla^2 E$ in Eq. (47). Then, in Section 4.2, we show how the results can be applied to develop efficient methods for linear systems embedded in the eigensolvers.

Numerical results show that the linear systems (39) are well-conditioned and M in (52) is an efficient preconditioner in solving linear system (51). This

leads to the robust and efficient eigensolvers for various geometric structure as shown in numerical examples.

Acknowledgements

The authors appreciate the anonymous referees for their useful comments and suggestion. This work is partially supported by the Ministry of Science and Technology, the Taida Institute of Mathematical Sciences, the Center for Advanced Study in Theoretical Sciences, and the National Center for Theoretical Sciences in Taiwan, and the ST Yau Center at NCTU.

References

[1] R.-L. Chern, C.-Chung Chang, Chien-C. Chang, and R.-R. Hwang. Numerical study of three-dimensional photonic crystals with large band gaps. *J. Phys. Soc. Japan*, 73:727–737, 2004.

[2] R.-L. Chern, H.-E. Hsieh, T.-M. Huang, W.-W. Lin, and W. Wang. Singular value decompositions for single-curl operators in three-dimensional Maxwell's equations for complex media. *SIAM J. Matrix Anal. Appl.*, 36:203–224, 2015. MR3316197

[3] C. Engström, C. Hafner, and K. Schmidt. Computations of lossy Bloch waves in two-dimensional photonic crystals. *J. Comput. Theor. Nanosci.*, 6:1–9, 2009.

[4] C. Engström and M. Wang. Complex dispersion relation calculations with the symmetric interior penalty method. *Int. J. Numer. Meth. Engng.*, 84:849–863, 2010. MR2762595

[5] P. G. Etchegoin, E. C. Le Ru, and M. Meyer. An analytic model for the optical properties of gold. *J. Chem. Phys.*, 125:164705, 2006.

[6] J. Gazalet, S. Dupont, J. C. Kastelik, Q. Rolland, and B. Djafari-Rouhani. A tutorial survey on waves propagating in periodic media: Electronic, photonic and phononic crystals. Perception of the Bloch theorem in both real and Fourier domains. *Wave Motion*, 50(3):619–654, 2013. MR3039547

[7] T.-M. Huang, W.-J. Chang, Y.-L. Huang, W.-W. Lin, W.-C. Wang, and W. Wang. Preconditioning bandgap eigenvalue problems in three dimensional photonic crystals simulations. *J. Comput. Phys.*, 229:8684–8703, 2010. MR2725369

[8] T.-M. Huang, H.-E. Hsieh, W.-W. Lin, and W. Wang. Eigendecomposition of the discrete double-curl operator with application to fast eigensolver for three dimensional photonic crystals. *SIAM J. Matrix Anal. Appl.*, 34:369–391, 2013. MR3046809

[9] T.-M. Huang, H.-E. Hsieh, W.-W. Lin, and W. Wang. Eigenvalue solvers for three dimensional photonic crystals with face-centered cubic lattice. *J. Comput. Appl. Math.*, 272:350–361, 2014. MR3227391

[10] T.-M Huang, W.-W. Lin, and W. Wang. A hybrid Jacobi-Davidson method for interior cluster eigenvalues with large null-space in three dimensional lossless Drude dispersive metallic photonic crystals. *Comput. Phys. Commun.*, 207:221–231, 2016. MR3541636

[11] Y.-L. Huang, T.-M. Huang, W.-W. Lin, and W.-C. Wang. A null space free Jacobi-Davidson iteration for Maxwell's operator. *SIAM J. Sci. Comput.*, 37(1):A1–A29, 2015. MR3296624

[12] K. Inoue and K. Ohtaka. *Photonic crystals: physics, fabrication and applications*, volume 94. Springer, 2004.

[13] J. D. Joannopoulos, S. G. Johnson, J. N. Winn, and R. D. Meade. *Photonic Crystals: Molding the Flow of Light*. Princeton University Press, Princeton, NJ, 2008.

[14] C. Kittel. *Introduction to solid state physics*. Wiley, New York, NY, 2005.

[15] Y. Liu and X. Zhang. Metamaterials: a new frontier of science and technology. *Chem. Soc. Rev.*, 40:2494–2507, 2011.

[16] M. Luo and Q. H. Liu. Three-dimensional dispersive metallic photonic crystals with a bandgap and a high cutoff frequency. *J. Opti. Soc. Amer. A*, 27(8):1878–1884, 2010.

[17] E. Moreno, D. Erni, and C. Hafner. Band structure computations of metallic photonic crystals with the multiple multipole method. *Phys. Rev. B*, 65:155120, 2002.

[18] J. B. Pendry, A. J. Holden, D. J. Robbins, and W. J. Stewart. Magnetism from conductors and enhanced nonlinear phenomena. *IEEE Trans. Microwave Theo. Tech.*, 47:2075–2084, 1999.

[19] J. B. Pendry, A. J. Holden, W. J. Stewart, and I. Youngs. Extremely low frequency plasmons in metallic mesostructures. *Phys. Rev. Lett.*, 76:4773–4776, 1996.

[20] A. Serdyukov, I. Semchenko, S. Tretyakov, and A. Sihvola. *Electromagnetics of Bi-anisotropic Materials: Theory and Applications*. Gordon and Breach Science, 2001.

[21] C. M Soukoulis. *Photonic crystals and light localization in the 21st century*, volume 563. Springer, 2001.

[22] A. Vial. Implementation of the critical points model in the recursive convolution method for modelling dispersive media with the finite-difference time domain method. *J. Opt. A: Pure Appl. Opt.*, 9:745–748, 2007.

[23] W. S. Weiglhofer and A. Lakhtakia. *Introduction to Complex Mediums for Optics and Electromagnetics*. SPIE, Washington, DC, 2003.

[24] K. Yee. Numerical solution of initial boundary value problems involving Maxwell's equations in isotropic media. *IEEE Trans. Antennas and Propagation*, 14:302–307, 1966.

Tsung-Ming Huang
Department of Mathematics
National Taiwan Normal University
Taipei 116
Taiwan
E-mail address: min@ntnu.edu.tw

Wen-Wei Lin
Department of Applied Mathematics
National Chiao Tung University
Hsinchu 300
Taiwan
E-mail address: wwlin@math.nctu.edu.tw

Weichung Wang
Institute of Applied Mathematical Sciences
National Taiwan University
Taipei, 106
Taiwan
E-mail address: wwang@ntu.edu.tw

Received September 18, 2018